Electronic Supplementary Material (ESI) for Polymer Chemistry.

<Supplementary Information>

High-performance non-volatile resistive switching memory based on a polyimide/graphene oxide nanocomposite

Ju-Young Cho[#a], Jeongjun Le[#b], Jihyun Jeon[b], Jaehyuk Im[b], Junhwan Jang[b], Seung-Won Jin[a], Hyeyoung Joung[a], Hwan-Chul Yu[a], Kyeong-Nam Nam[a], Hyeong-Joo Park[a], Dong-Min Kim[a], In-Ho Song[a], Jaesung Yang[a], Soohaeng Cho[b], and Chan-Moon Chung[a]**

[a]Department of Chemistry, Yonsei University, Wonju, Gangwon-do 26493, Republic of Korea

[b]Department of Physics, Yonsei University, Wonju, Gangwon-do 26493, Republic of Korea

1. Characterization of GO-AnDA, PAA-GO, neat-PI and PI-GO

1.1 Characterization of GO-AnDA

A high-resolution XPS was used to measure the surface composition and functional groups of GO and GO-AnDA based on the chemical shift observations. The high resolution C1s XPS spectra of GO and GO-AnDA are presented in Fig. S1a and S1b, respectively. As shown in Fig. S1a, the C1s XPS spectrum of the pristine GO indicated that the GO possesses a significant degree of oxidation based on the observation of numerous oxygen-containing groups such as alcohols (C–OH), epoxides (C–O–C), and carbonyls (–O–C=O–).[17,S1-S3] These oxygen functional groups mean that GO has the potential for further chemical modification. Compared with GO, the C1s XPS spectra of GO-AnDA showed a significant decrease in epoxide groups (287.2 eV). An additional peak at 285.4 eV in the C1s XPS spectra of GO-AnDA originated from the C–N bonds. These results indicate that the AnDA binds to the surface of GO through a nucleophilic attack between the amine groups of AnDA and the epoxide groups on the GO surface.[S1-S4] Thus, the AnDA was successfully grafted to the epoxide groups of GO.

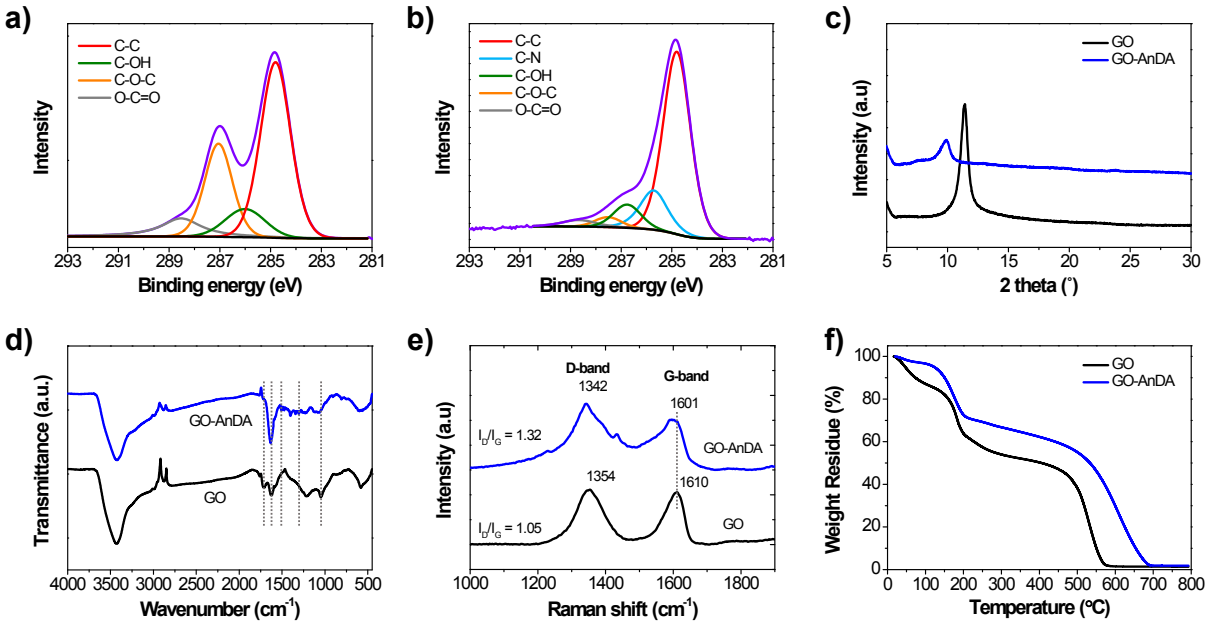

Fig. S1 C1s XPS spectra of a) GO and b) GO-AnDA. c) XRD spectra, d) FT-IR spectra, e) Raman spectra, and f) TGA thermograms of GO and GO-AnDA.

The GO and GO-AnDA structures were further investigated by XRD, and the spectra are shown in Fig. S1c. XRD analysis was used to determine the interlayer distance in nanosheets of GO and GO-AnDA. The XRD pattern of GO exhibited a sharp diffraction peak at 11.42°, corresponding to an interlayer d-spacing of 7.74 Å. After modification with AnDA, the GO-AnDA showed a diffraction peak at 9.90°, corresponding to an interlayer d-spacing of 8.93 Å. The diffraction peak of GO-AnDA significantly shifted to a smaller angle region compared to that of GO. The higher GO-AnDA interlayer d-spacing compared to GO implies that GO was modified with AnDA.[S5,S6]

The chemical structures of GO and GO-AnDA were confirmed by FT-IR, and the spectra are shown in Fig. S1d. The FT-IR spectrum of GO exhibited three characteristic bands at 1715, 1625, and 1050 cm^{-1}, which correspond to carboxyl C=O, C=C skeleton and epoxy C-O-C stretching vibrations, respectively.[28,S4,S6] After modification, GO-AnDA showed absorption bands at 1509 and 1306 cm^{-1} due to N-H bending and C-N stretching of secondary aromatic amines, respectively.[28,S4] The relative intensity of the epoxy C-O-C stretch of GO-AnDA at 1050 cm^{-1} significantly decreased compared to GO. This result clearly confirmed the C-N bond formation between amine groups of AnDA and the epoxy groups of GO.

In addition, the Raman spectra of GO and GO-AnDA are given in Fig. S1e. The pristine GO shows a typical Raman band (so-called G-band) around at 1610 cm^{-1} due to the E_{2g} phonon of the sp^2 hybridized carbon atom of graphite. The so-called D-band was observed at about 1350 cm^{-1} and is associated with structural defects.[S7-S9] The intensity ratio (ID/IG) of the D-band (ID) and the G-band (IG) indicates the amount of defects and disorder in the graphite structure.[S7,S10] The ID/IG of the G-band of GO-AnDA increased from 1.05 to 1.32. This indicates that the ordered structure of GO has been disrupted by the introduction of AnDA.

Thermal decomposition of the GO and GO-AnDA samples was studied by thermogravimetric analysis (TGA) under a nitrogen atmosphere, and their TGA thermograms are presented in Fig. S1f. The thermogram of GO exhibited three major weight losses.[28,S11-S13] The first weight loss occurred at around 45°C due to the loss of residual H_2O contained in GO, while the second weight loss occurred at around 180°C due to the decomposition of unstable oxygen-containing functional groups such as epoxy, hydroxyl, and carboxyl groups. [28,S11,S14] The last weight loss around 530°C was ascribed to the removal of more stable oxygen functionalities.[S12,S15] Compared to GO, GO-AnDA showed higher thermal stability due to the substitution of amine groups for oxygen groups.[28,S16,S17] The TGA thermograms also indicate that the GO surface was modified by AnDA.

1.2 Characterization of PAA-GO, neat-PI and PI-GOs

TGA and DSC were conducted to investigate the thermal stability of the neat-PI and PI-GOs. Fig. S2a shows the TGA thermograms of neat-PI and PI-GOs. The neat-PI and PI-GOs showed high thermal stability up to 500°C. The thermal stability of PI-GOs increased with increasing GO content at higher temperature. The thermal decomposition of PI begins with chain cleavage and radical formation, and thus the carbon surface of the GO sheets in the PI matrix might act as a radical scavenger to retard thermal degradation.[S4,S18] The high thermal stability can also be attributed to strong covalent adhesion between the GO and PI matrix.[S6,S19] As shown in Fig. S2b, the glass transition temperature (T_g) of the PI-GO composites increased with increasing GO content; the T_g values of neat-PI and the PI-GOs containing 0.1, 1.5, and 3 wt% GO were 387, 391, 395, and 403°C, respectively. These results indicate that the existence of covalently bonded GO might increase the rigidity of the PI chains, and thus restrict their thermal motion.[S20-S23]

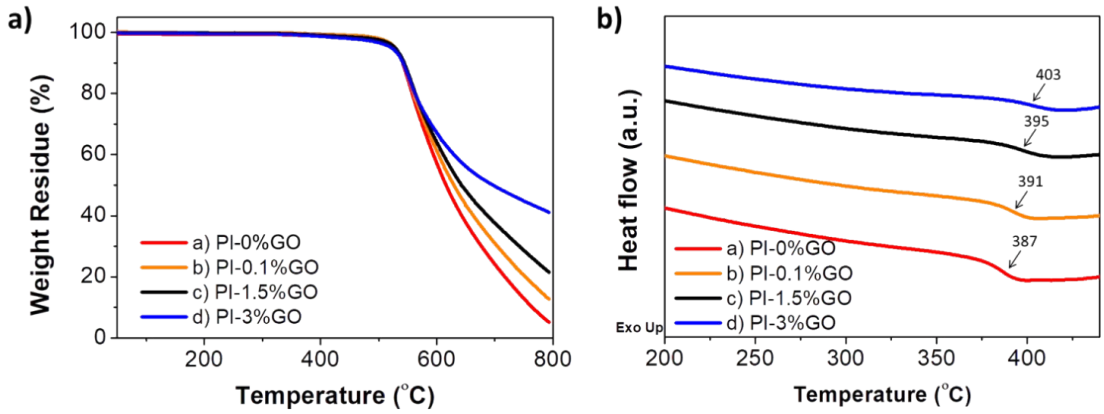

Fig. S2 a) TGA and b) DSC thermograms of the PI-GOs containing 0 wt% (neat-PI), 0.1 wt%, 1.5 wt%, and 3 wt% GO.

2. Characteristics of PI-GO based memory devices (part 1)

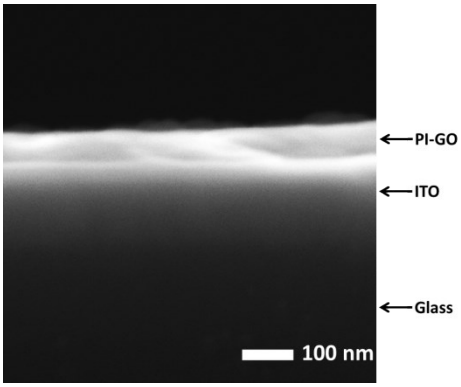

Fig. S3 SEM image of a cross section of PI-1.5%GO/ITO glass.

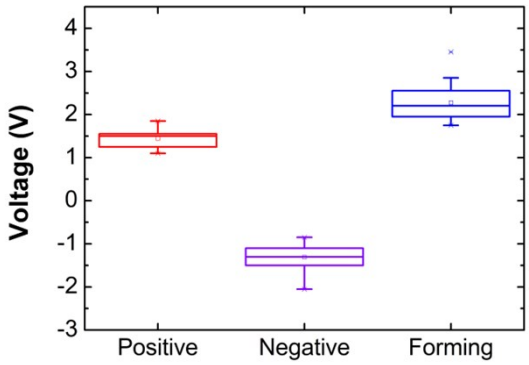

Fig. S4 The statistical distributions of sweeping and forming voltages of the Al/PI-1.5%GO/ITO device.

3. Isothermal TGA measurement of PI-GO

Isothermal TGA experiments were carried out for PI-1.5%GO under ambient atmosphere. The TGA chamber was quickly heated up to 415°C and held there for 5 min. The dynamic TGA curve shown in Fig. S4 indicates that only very slight weight loss occurred at 415°C for 5 min. This indicates that any moisture, residual solvent or low molecular weight material was removed during the thermal annealing.

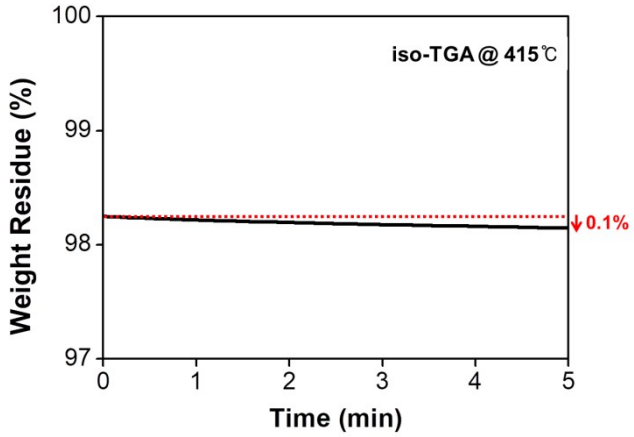

Fig. S5 Isothermal TGA thermogram of the PI-1.5%GO at 415°C for 5 min.

4. Characteristics of PI-GO based memory devices (part 2)

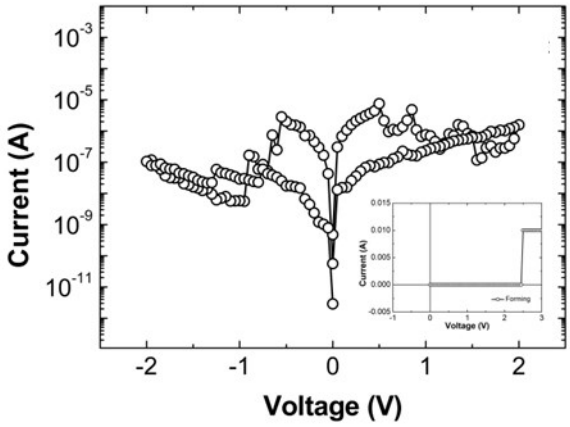

Fig. S6 I-V characteristic of the Al/PI-1.5%GO/ITO device (with UV-Ozone treatment and without post-annealing).

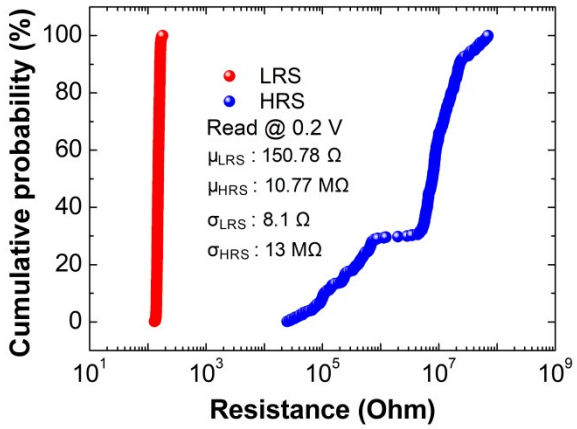

Fig. S7 Cumulative probability distribution of LRS and HRS resistance.

5. Molecular simulation

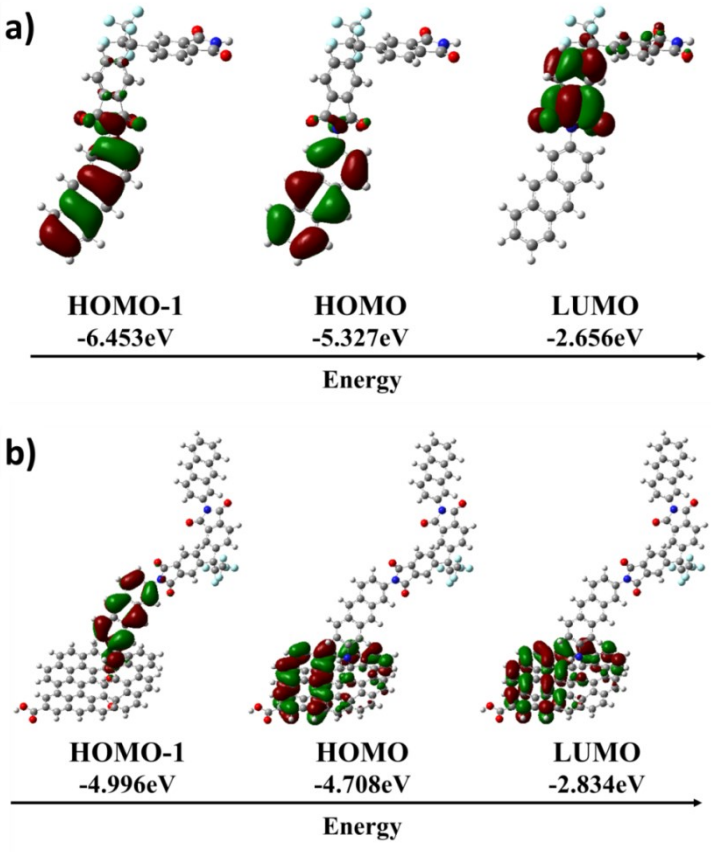

Fig. S8 Calculated frontier molecular orbitals of basic unit a) neat-PI and b) PI-GO.

6. References

S1. J.-Y. Wang, S.-Y. Yang, Y.-L. Huang, H.-W. Tien, W.-K. Chin and C.-C. M. Ma, *J. Mater. Chem.*, 2011, **21**, 13569

S2. W.-H. Liao, S.-Y. Yang, S.-T. Hsiao, Y.-S. Wang, S.-M. Li, C.-C. M. Ma, H.-W. Tien and S.-J. Zeng, *ACS Appl. Mater. Interfaces*, 2014, **6**, 15802.

S3. Y. Li, X. Pei, B. Shen, W. Zhai, L. Zhang, W. Zheng, *RSC Adv.*, 2015, **5**, 24342.

S4. J. Dong, C. Yin, X. Zhao, Y. Li and Q. Zhang, *Polymer*, 2013, **54**, 6415.

S5. K. Krishnamoorthy, M. Veerapandian, K. Yun and S. J. Kim, *Carbon*, 2013, **53**, 38.

S6. K.-M. Jeong, Y.Li , D.-G. Yoo, N.-K. Lee, H.-G. Lee, S. Ando and C.-S. Ha, *Polym. Inter.*, 2018, **67**, 588.

S7. K. Sarkar, G. Madras and K. Chatterjee, *RSC Adv.*, 2015, **5**, 50196.

S8. L. Zhao, W. Gu, C. Zhang, X. Shi and Y. Xian, *J. Colloid Interface Sci.*, 2016, **465**, 279.

S9. G. R. P, S. R. V, A. Kanwat and J. Jang, *Mater. Res. Bull.*, 2016, **74**, 346.

S10. L. G. Cançado, A. Jorio, E. H. M. Ferreira, F. Stavale, C. A. Achete, R. B. Capaz, M. V. O. Moutinho, A. Lombardo, T. S. Kulmala and A. C. Ferrari, *Nano Lett.*, 2011, **11**, 3190.

S11. G. Yu and P. Wu, *Polym. Chem.*, 2014, **5**, 96.

S12. S. Ramakrishnan, M. Dhakshnamoorthy, E. Jelmy, R. Vasanthakumari and N. K. Kothurkar, *RSC Adv.*, 2014, **4**, 9743.

S13. P. Song, X. Zhang, M. Sun, X. Cui and Y. Lin, *RSC Adv.*, 2012, **2**, 1168.

S14. K. Zhang, L. L. Zhang, X. Zhao and J. Wu, *Chem. Mater.*, 2010, **22**, 1392.

S15. G. M. Neelgund, A. Oki and Z. Luo, *Mater. Res. Bull.*, 2013, **48**, 175.

S16. B. Dehghanzad, M. K. R. Aghjeh, O. Rafeie, A. Tavakoli and A. J. Oskooie, *RSC Adv.*, 2016, **6**, 3578.

S17. A. Navaee and A. Salimi, *RSC Adv.*, 2015, **5**, 59874.

S18. H. W. Ha, A. Choudhury, T. Kamal, D.-H. Kim and S.-Y. Park, *ACS Appl. Mater. Interfaces*, 2012, **4**, 4623.

S19. C. Wang, Y. Lan, W. Yu, X. Li, Y. Qian and H. Liu, *Appl. Surf. Sci.*, 2016, **362**, 11.

S20. J. Zhu, S. Wei, X. Chen, A. B. Karki, D. Rutman, D. P. Young and Z. Guo, *J. Phys. Chem. C*, 2010, **114**, 8844.

S21. D. Ding, X. Yan, X. Zhang, Q. He, B. Qiu, D. Jiang, H. Wei, J. Guo, A. Umar, L. Sun, Q. Wang, M. A. Khan, D. P. Young, X. Zhang, B. Weeks, T. C. Ho, Z. Guo and S. Wei, *Superlattices Microstruct.*, 2015, **85**, 305.

S22. Y. Guo, G. Xu, X. Yang, K. Ruan, T. Ma, Q. Zhang, J. Gu, Y. Wu, H. Liu and Z. Guo, *J. Mater. Chem. C*, 2018, **6**, 3004.

S23. D. Zhao, G. Zhu, Y. Ding and J. Zheng, *Polymers*, 2018, **10**, 716.